Modelling of semiconductor nanostructured devices within the tight-binding approach

1999 J. Phys.: Condens. Matter 11 6035

(http://iopscience.iop.org/0953-8984/11/31/311)

J. Phys.: Condens. Matter **11** (1999) 6035–6043. Printed in the UK PII: S0953-8984(99)01394-6

Modelling of semiconductor nanostructured devices within the tight-binding approach

Paolo Lugli, Aldo Di Carlo† and Andrea Reale

INFM—Dipartimento di Ingegneria Elettronica, Università di Roma 'Tor Vergata', Via di Tor Vergata, 110, 00133 Roma, Italy

E-mail: dicarlo@ing.uniroma2.it

Received 29 January 1999

Abstract. A self-consistent tight-binding approach applied to semiconductor nanostructures is presented. This allows us to describe electronic and optical properties of nanostructured devices beyond the usual envelope function approximation. Examples of applications are given for high-electron-mobility transistors and semiconductor optical amplifiers.

1. Introduction

Modern microelectronics and optoelectronics are heavily based upon semiconductor nanostructures, where the dimension of the 'active' region is in the nanometric range. Typical examples are the high-electron-mobility transistor (HEMT), the semiconductor laser, and semiconductor optical amplifiers (SOAs). A basic element of all of these structures is a heterojunction between different semiconductor materials.

The theoretical study of electronic and optical properties of such devices has been undertaken by different methods. These range from *ab initio* approaches [1], which are very precise but require a large computational effort and, consequently, can only be applied to very small nanostructures, to approximate but easy-to-handle and fast methods such as those based on the $\boldsymbol{k} \cdot \boldsymbol{p}$ expansion in the envelope function approximation (EFA) [2]. In its simplest form, the EFA leads to the evaluation of the energy levels of nanosystems by simply solving a one-electron Schrödinger equation where each semiconductor is described in terms of effective masses and band edges [3]. Despite its ready applicability, the EFA method is limited by several factors. First of all, it is not capable of describing the nanosystem over the whole Brillouin zone. Second, the use of the same periodic part of the Bloch function for all of the semiconductors forming the heterojunction makes the EFA inapplicable to very thin structures. Moreover, the level of description needed to account for and to predict the properties of last-generation microelectronic and optoelectronic devices cannot be reached within the context of simple EFA methods.

The empirical tight-binding (TB) method [4] has been shown to be a valid alternative to the EFA method, since it improves the physical content of the description of the nanostructure with respect to that from the EFA without requiring a much higher computational effort. In particular, it allows us to treat indirect-gap semiconductors, and heterostructures formed by indirect and direct materials, and to describe very thin layers [5–8].

† Author to whom any correspondence should be addressed.

0953-8984/99/316035+09$30.00

The TB method has been mainly used in the calculation of the electronic properties of nanostructures without taking into account self-consistent charge redistribution, which is an important requirement when we deal with real systems. However, very recently, we have shown [9] that a self-consistent tight-binding procedure can be defined.

In this paper we will describe the self-consistent TB model and its application to the study of the electronic and optical properties of realistic nanostructures.

2. Theory

In this section we discuss the self-consistent tight-binding model for a system in which the translational symmetry is broken in one direction—for example, along the growth axis (z). The wave function $|E, \boldsymbol{k}_\parallel\rangle$ can be written as linear combination of planar Bloch sums, $|\alpha, m, \boldsymbol{k}_\parallel\rangle$ [7, 10]:

$$|E, \boldsymbol{k}_\parallel\rangle = \sum_{\alpha,m} C_{\alpha,m}(E, \boldsymbol{k}_\parallel)|\alpha, m, \boldsymbol{k}_\parallel\rangle \tag{1}$$

with

$$|\alpha, m, \boldsymbol{k}_\parallel\rangle = \frac{1}{\sqrt{N}} \sum_{\boldsymbol{R}^m_{\alpha\parallel}} \mathrm{e}^{\mathrm{i}\boldsymbol{k}_\parallel \cdot \boldsymbol{R}^m_{\alpha\parallel}} |\alpha, \boldsymbol{R}_\alpha\rangle \tag{2}$$

where $|\alpha, \boldsymbol{R}_\alpha\rangle$ is a localized orbital, $\boldsymbol{k}_\parallel$ is the in-plane wave vector, and N is the number of unit cells in the atomic plane. The subscript α refers both to the basis-atom index and to the atomic orbital index. The lattice vector, $\boldsymbol{R}_\alpha = \boldsymbol{R} + \boldsymbol{v}_\alpha$ (where $\boldsymbol{v}_\alpha$ is the basis-atom displacement), can be written as $\boldsymbol{R}_\alpha = m\boldsymbol{d} + \boldsymbol{R}^m_{\alpha\parallel}$ where m is an integer, $\boldsymbol{d}$ a vector parallel to the growth direction with modulus equal to the distance between two atomic planes, and $\boldsymbol{R}^m_{\alpha\parallel}$ is a vector on the mth atomic plane. For a given $\boldsymbol{k}_\parallel$, the eigenstates E are calculated by solving the secular equation $(H + V_\mathrm{H})|E, \boldsymbol{k}_\parallel\rangle = E|E, \boldsymbol{k}_\parallel\rangle$ where H is the system tight-binding Hamiltonian and V_H is the Hartree potential. The influence of the electronic charge rearrangement can be included at a Hartree level by solving the Poisson equation, $\mathrm{d}^2V_\mathrm{H}/\mathrm{d}z^2 = -\rho(z)/\varepsilon$, where ε is the static dielectric constant. The charge density in the mth plane $\rho(m)$ is defined by

$$\rho(m) = -\frac{e}{(2\pi)^2} \int_{\mathrm{BZ}_\parallel} \mathrm{d}\boldsymbol{k}_\parallel \sum_{n,\alpha} \left|C_{n,\alpha}(E_n, \boldsymbol{k}_\parallel)\right|^2 \tilde{f}(E_n, E_\mathrm{F}) \tag{3}$$

where e is the electron charge and n labels the energy levels for a given $\boldsymbol{k}_\parallel$. The function $\tilde{f}(E_n, E_\mathrm{F})$ is defined as follows:

$$\tilde{f}(E_n, E_\mathrm{F}) = \begin{cases} f(E_n, E_\mathrm{F}) & \text{for the conduction states} \\ 1 - f(E_n, E_\mathrm{F}) & \text{for the valence states} \end{cases} \tag{4}$$

where $f(E_n, E_\mathrm{F})$ is the Fermi distribution function with a given Fermi level E_F. $\tilde{f}(E_n, E_\mathrm{F})$ is a well behaved function which is different from zero only in the proximity of the valence and conduction band edges. In order to evaluate the carrier density (equation (3)), a full $\boldsymbol{k}_\parallel$-integration is performed in the 2D Brillouin zone ($\mathrm{BZ}_\parallel$) by using the special-k-points technique in the irreducible wedge [11]. The convergence of this integration has been obtained by using five special points with $|\boldsymbol{k}_\parallel| \leqslant 0.062\pi/a$ for direct-band-gap material. To achieve self-consistency for indirect-band-gap material we use eight points with $|\boldsymbol{k}_\parallel| \leqslant 0.22\pi/a$.

The Poisson and Schrödinger equations in the TB representation are iteratively solved until convergence is reached. Open-chain (infinite-well) boundary conditions are used for the Schrödinger equation. In order to avoid them having any influence on the calculated electronic levels, boundaries are chosen far away from the nanostructure's active region. This

may not be satisfactory for high-energy states such as those above the barrier. Indeed, a better choice for the boundary condition is provided by applying the scattering theory as explained in reference [10]. However, for all of the situations discussed here the open-chain condition represents a valid choice. Moreover, the use of an open-chain boundary condition induces the Hamiltonian matrix to have a 'band' form. This implies that very efficient diagonalization methods, suited to this matrix form, can be applied. We have here introduced a hybrid method to diagonalize the tight-binding Hamiltonian which uses a standard (LAPACK [12]) routine to calculate eigenvalues and an inverse iteration scheme [13] to calculate eigenvectors. The advantage of this procedure relies on the fact that only a few eigenvectors are needed, namely those close to the energy band gap. To speed up the self-consistent TB calculation, we take as the initial starting potential the one obtained self-consistently in the effective-mass approximation.

When optical properties are of interest, one can make use of the Kubo formula to define the susceptibility tensor which is related to the current–current response function of the electromagnetic perturbation. This can be easily calculated within the tight-binding scheme *without* introducing new fitting parameters [14]. If we consider a linear polarization of the light along the ith axis, the absorption coefficient can be written as [9, 14]

$$\alpha(\omega) = \frac{4\pi^2}{nc\omega S} \sum_{E,E',\boldsymbol{k}_\parallel} \left[f(E) - f(E')\right] \delta(\hbar\omega + E - E') \left| \langle E, \boldsymbol{k}_\parallel | \sum_{\alpha,m} J_i(\alpha, m) | E', \boldsymbol{k}_\parallel \rangle \right|^2 . \tag{5}$$

Here, S is the transverse area of the primitive cell, n is the refractive index, and c is the speed of light. The matrix elements of the current operator can be expressed as

$$\begin{aligned} \langle E, \boldsymbol{k}_\parallel | \boldsymbol{J}(\alpha, m) | E', \boldsymbol{k}_\parallel \rangle = {} & \frac{S}{N} \sum_{\substack{\alpha',m' \\ \alpha'',m''}} C^*_{\alpha',m'}(E, \boldsymbol{k}_\parallel) C_{\alpha'',m''}(E', \boldsymbol{k}_\parallel) \\ & \times \sum_{\boldsymbol{R}^m_{\alpha\parallel}, \boldsymbol{R}^{m'}_{\alpha'\parallel}, \boldsymbol{R}^{m''}_{\alpha''\parallel}} \mathrm{e}^{\mathrm{i}\boldsymbol{k}_\parallel \cdot (\boldsymbol{R}^{m''}_{\alpha''} - \boldsymbol{R}^{m'}_{\alpha'})} \langle \alpha', \boldsymbol{R}_{\alpha'} | \boldsymbol{j}(\alpha, \boldsymbol{R}_\alpha) | \alpha'', \boldsymbol{R}_{\alpha''} \rangle \end{aligned} \tag{6}$$

where

$$\begin{aligned} & \langle \alpha', \boldsymbol{R}_{\alpha'} | \boldsymbol{j}(\alpha, \boldsymbol{R}_\alpha) | \alpha'', \boldsymbol{R}_{\alpha''} \rangle \\ & \qquad = \frac{\mathrm{i}e}{2\hbar d S} t_{\alpha',\alpha''}(\boldsymbol{R}_{\alpha'} - \boldsymbol{R}_{\alpha''}) [\boldsymbol{R}_{\alpha'} - \boldsymbol{R}_{\alpha''}] \left\{ \delta_{\alpha' \boldsymbol{R}_{\alpha'}, \alpha \boldsymbol{R}_\alpha} + \delta_{\alpha'' \boldsymbol{R}_{\alpha''}, \alpha \boldsymbol{R}_\alpha} \right\} . \end{aligned}$$

Here $t_{\alpha',\alpha''}(\boldsymbol{R}_{\alpha'} - \boldsymbol{R}_{\alpha''}) = \langle \alpha', \boldsymbol{R}_{\alpha'} | H | \alpha'', \boldsymbol{R}_{\alpha''} \rangle$ is the tight-binding hopping matrix element.

The $\boldsymbol{k}_\parallel$-integration needed to calculate the luminescence or absorption coefficient (equation (5)) is performed in the irreducible wedge of the 2D Brillouin zone. Since we are only interested in calculating these optical properties close to the energy gap, we limited the integration to the region $|\boldsymbol{k}_\parallel| < 0.12\pi/a$.

In order to be able to change the carrier distribution function without recalculating all of the eigenvalues/eigenvectors of the Hamiltonian, we first calculate (and store) the energy levels and the squared optical matrix elements for each $\boldsymbol{k}_\parallel$. We then evaluate the luminescence or the absorption coefficient by performing the sums in equation (5). To reduce the numerical fluctuation induced by a finite number of $\boldsymbol{k}_\parallel$-points being considered ($\sim$1600), we sum over a much finer $\boldsymbol{k}_\parallel$-grid ($\sim 10^5$ points). Energy levels and squared matrix elements at these new $\boldsymbol{k}_\parallel$-points are obtained by using a bilinear interpolation of the calculated quantities. This is allowed since the variations of both the energy levels and the squared matrix elements in the irreducible wedge are quite smooth. Strain is included in the TB model by scaling the hopping matrix elements by using the modified Harrison scaling law [15]. The tight-binding parameters are adapted from reference [7].

3. Results

Self-consistent TB approaches are of great interest as regards those devices whose characteristics depend on the properties of the energy dispersion over the whole Brillouin zone. Then, traditional methods like effective-mass approximation or the $\boldsymbol{k} \cdot \boldsymbol{p}$ method, which are limited in their validity to the surroundings of the Γ valley, are not applicable.

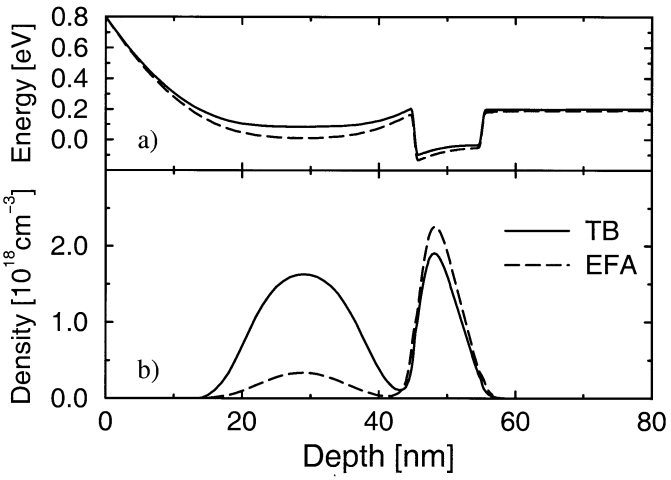

Figure 1. (a) The self-consistent band profile of a $Al_{0.45}Ga_{0.55}As/GaAs/Al_{0.3}Ga_{0.7}As$ HEMT structure. (b) The self-consistent charge density of the HEMT.

This is for instance the case for GaAs/AlGaAs HEMTs, for which mixing between different bands occurs. $Al_{1-x}Ga_xAs$ remains a direct-band-gap material up to an Al concentration of about 40%. We have investigated the performance degradation when a parasitic channel forms by accumulation of carriers in the X valley, with the Al concentrations of the cap layer chosen to give $E_\Gamma = E_X$. It becomes evident (see figure 1) that the EFA completely fails to describe the charge redistribution between the 2D channel and the parasitic channel which forms due to the large X-valley contribution to the charge density.

In order to confirm that the self-consistency is achieved regardless of the type of energy gap, the self-consistent TB approach can be also used for Si/SiGe devices for which conventional device simulators are unable to describe the electronic properties [16]. Figure 2(a) and figure 2(b) show respectively the valence band profile and charge density of a p-type SiGe/Si MODFET. Strain is responsible for the splitting of the heavy- and light-hole bands. The charge densities obtained by the TB and EFA methods are very different. This is mainly due to the high non-parabolicity and anisotropy of the valence band.

3.1. Electroluminescence of pseudomorphic HEMT

In this section we show how the tight-binding approach can be coupled to conventional Monte Carlo simulation of charge transport in pseudomorphic HEMTs (P-HEMTs) in order to reproduce the electroluminescence spectra observed when the device is biased in near-breakdown conditions. Indeed, near the breakdown, the presence of electrons and holes in the P-HEMT channel opens the way for radiative recombination processes leading to band edge electroluminescence.

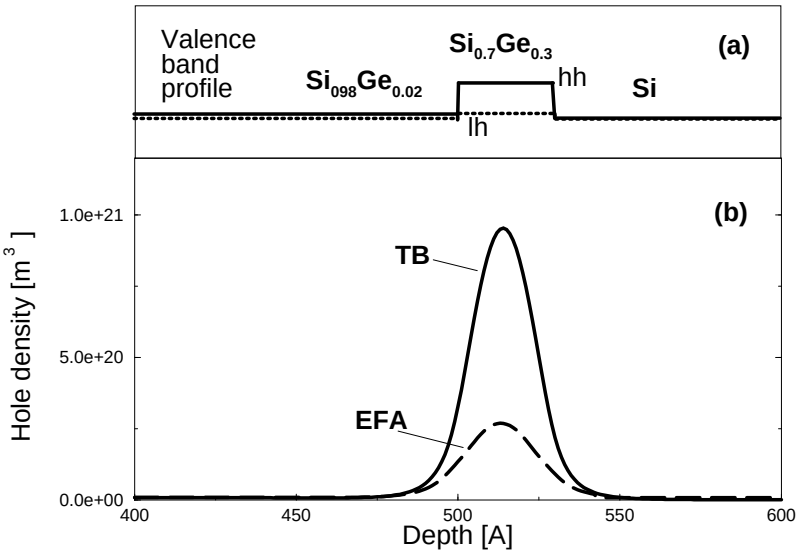

Figure 2. The valence band profile (a) and charge density (b) of a $Si_{0.98}Ge_{0.02}/Si_{0.7}Ge_{0.3}/Si$ p-channel MODFET structure.

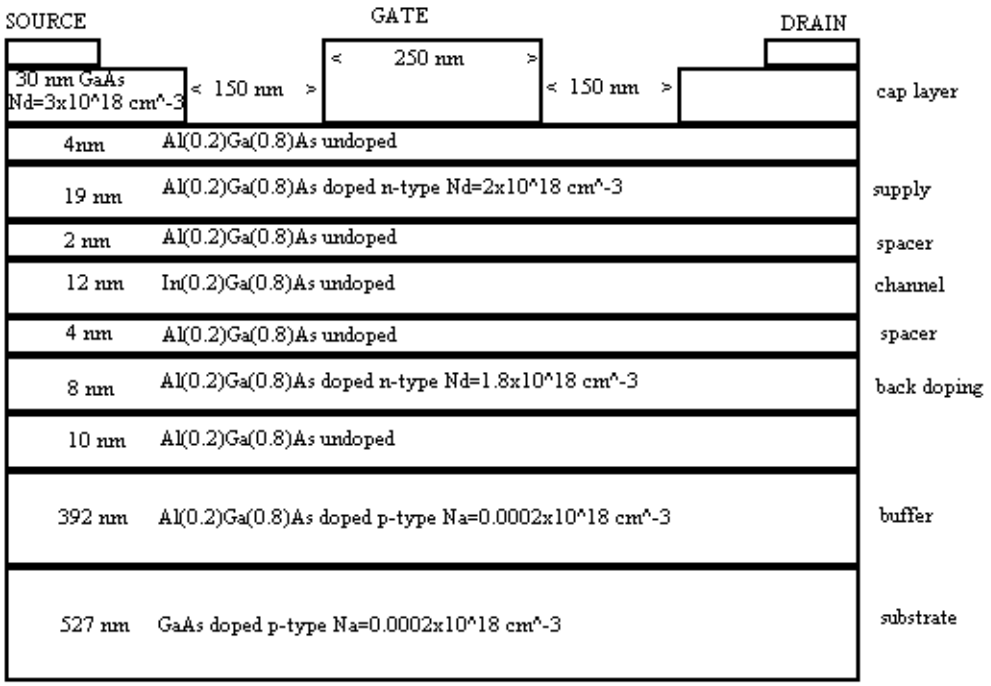

Figure 3. A schematic representation of the simulated device.

We have developed a Monte Carlo code to simulate hot-carrier effects in P-HEMTs. The modulation-doped P-HEMT structure of figure 3 is typical for P-HEMTs, which are devices of great importance in the microwave field [3].

Delta doping is used in the upper as well as in the lower barrier. Ohmic contacts are simulated by two highly doped regions that penetrate from source and drain pads directly into the channel region. The dimension of the channel (120 Å) allows for quantization of the electronic levels.

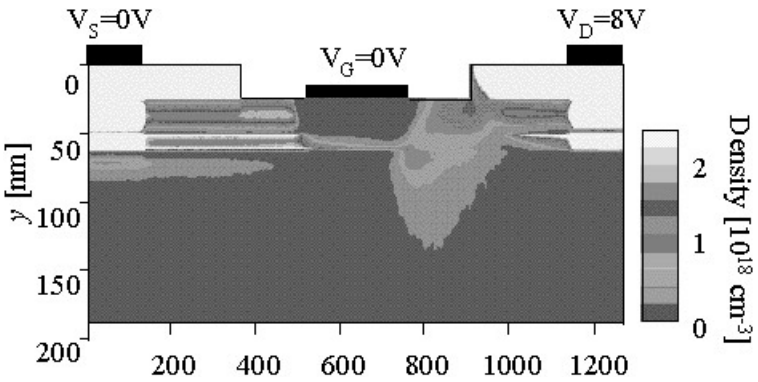

Figure 4. The electron density in the simulated HEMT.

Under bias conditions close to the breakdown of the device, the electrons gain energy from the field and are able to move to upper valleys close to the gate–drain region. Since in the upper valley the effective mass is higher, the electrons lose velocity, and consequently the carrier density increases as shown in figure 4. At the same time, since the potential energy is high, electrons are able to generate holes via the impact ionization processes. The generated holes can radiatively recombine with electrons (electroluminescence).

By using the distribution function as obtained by the MC simulation and the TB calculation for the calculation of the quantized levels and the optical matrix elements for interband transitions, we are able to calculate the electroluminescence spectra of the HEMT. The calculated electroluminescence spectrum, for $T = 195$ K, as a function of the emission energy, is shown in figure 5 together with the hole density. The picture shows the accumulation of holes under the gate and in the gate–source region. Indeed, holes created in the gate–drain region are swept back from the electric field and reach the gate–drain region, where they stop since the electric field there is quite low. Since the HH quantized levels are now above the LH states, the luminescence transitions occur between conduction levels and the heavy-hole levels. The electroluminescence is composed of a broad peak at around 1.3 eV and two other minor peaks close to 1.35 eV. The main peak corresponds to the $C_1 \rightarrow HH_1$ transition,while the other two peaks are related to the $C_2 \rightarrow HH_1$ and $C_2 \rightarrow HH_2$ transitions. We observe that the bias-induced bending of the quantum well forming the channel allows radiative recombinations of electrons and holes even from levels normally forbidden under flat-band conditions. Indeed, the C2 $\rightarrow$ HH1 transition is forbidden for a flat infinite-barrier quantum well [2], but becomes allowed when the well is distorted by the band bending [9]. Furthermore, we observe that the emitted light is mainly polarized in the in-plane direction, since the levels have essentially a heavy-hole character.

3.2. Optical properties of semiconductor optical amplifiers

The reference structure for our study consists of an $In_{0.533}Ga_{0.467}As$ quantum well 153 Å wide (52 monolayers) surrounded by $In_{0.74}Ga_{0.26}As_{0.56}P_{0.44}$ barriers, lattice matched to an InP substrate. We investigate the differences in optical matrix elements and eventually the gain

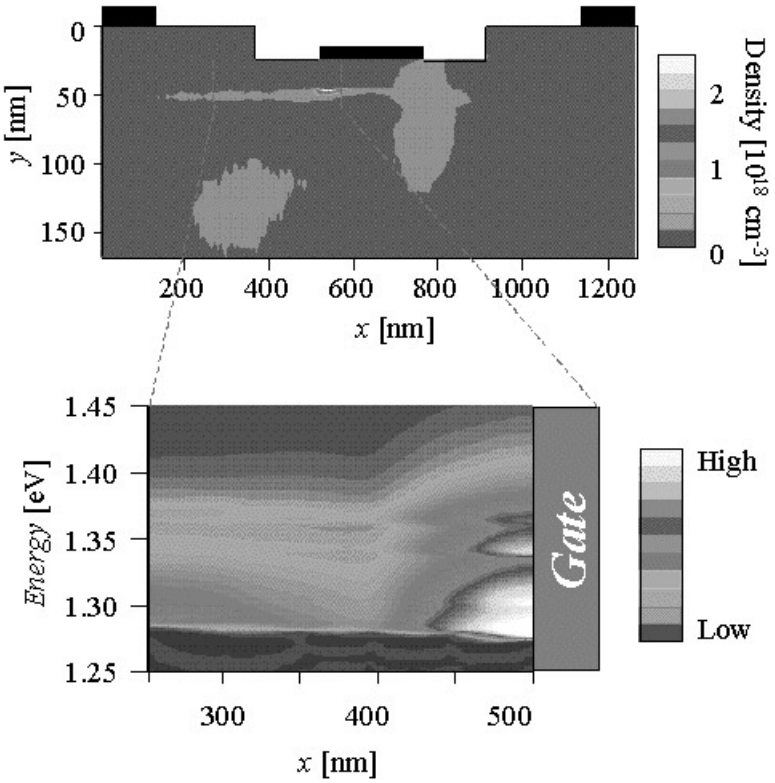

Figure 5. The hole density and the electroluminescence spectrum for the simulated HEMT.

coefficient for the reference structure compared to one for which three monolayers (ML) of InGaAs in the middle of the well are replaced by strained GaAs.

The latter system has been shown to guarantee a good degree of polarization insensitivity for multiple-quantum-well SOAs (MQW-SOAs) [17, 18], since the inner monolayers of GaAs in the well act as a strong tensile strain perturbation of the valence band states in the MQW active region. The polarization independence is achieved because the δ-strain enhances the light-hole–conduction band transition; by selection rules, this means an enhanced TM mode contribution to the overall material gain. This allows the modes propagating into the fibre to experience the same optical gain, regardless of their polarization (TM or TE).

The gain coefficient can be calculated from equation (5) with an appropriate choice of the quasi-Fermi levels. Those are obtained by explicitly considering charge injection from the contacts. We simulated the real structure of the device within a drift-diffusion scheme, solved self-consistently with the Poisson equation, in order to evaluate the position of the quasi-Fermi levels with sufficiently accurate precision.

The calculated gain coefficients for the well with and without GaAs δ-strain are shown in figure 6(b) and figure 6(a), respectively. It can be seen that there is an appreciable difference for the TE and TM polarizations for the system without the δ-strain, both in intensity and energy threshold. With δ-strain at the same time, the threshold difference between the two polarizations is removed, and the TM contribution is stronger than the TE one at all of the energies (or wavelengths) of interest around the 1.55 μm window. The sharp peak observed in the TM gain is due to negative mass effects in the first light-hole subband [17].

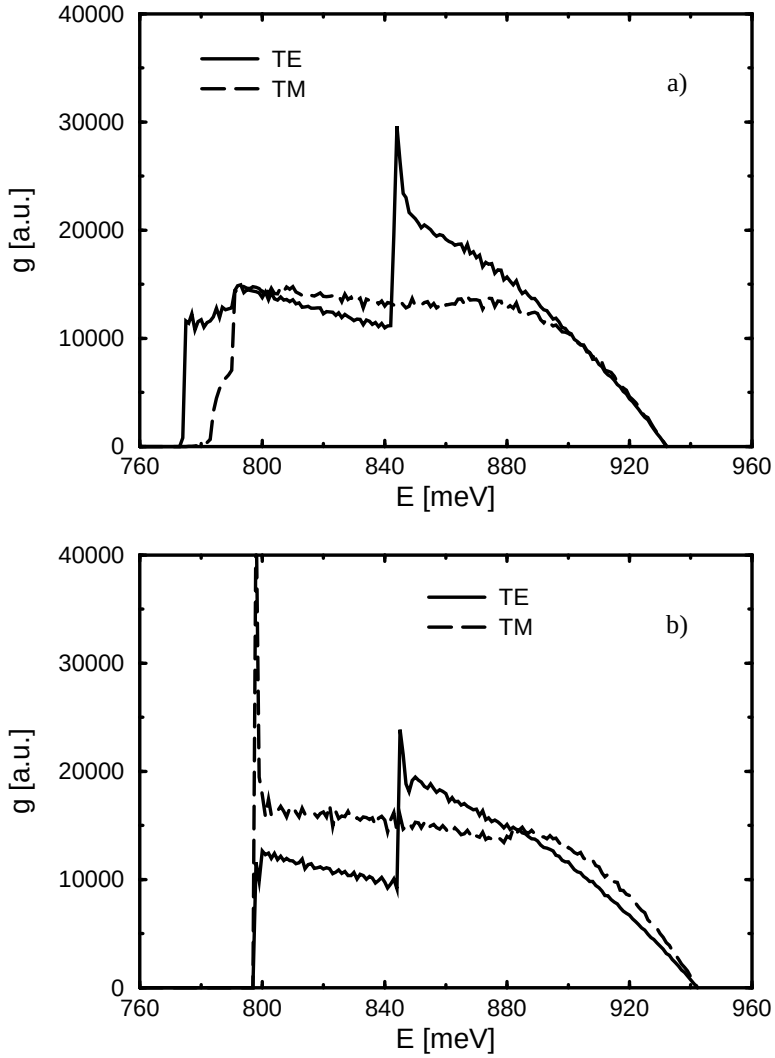

Figure 6. The gain coefficients for the SOA (a) without and (b) with δ-strain.

4. Conclusions

We have shown that a self-consistent tight-binding approach can be used to evaluate the electronic structure and optical properties of semiconductor nanostructures. This represents a further step, with respect to the envelope function model, towards an *ab initio* calculation of such properties.

Acknowledgments

We acknowledge the support of CSELT, MURST, and of the European Commission through the TMR Network 'Ultrafast Quantum Electronics'.

References

[1] Wood D M, Wei S-H and Zunger A 1988 *Phys. Rev.* B **37** 1342
Park C H and Chang K J 1993 *Phys. Rev.* B **47** 12 709
[2] Bastard G 1988 *Wave Mechanics Applied to Semiconductor Heterostructures* (Les Ulis: Les Editions de Physique)
[3] Morkoç H, Unlu H and Ji G 1991 *Principles and Technology of MODFETS* (Chichester: Wiley)
[4] Slater J C and Koster G F 1954 *Phys. Rev.* **94** 1498
Bullet D W 1980 *Solid State Physics* vol 35 (New York: Wiley) p 129
Majewski J A and Vogl P 1989 *The Structure of Binary Compounds* ed F R de Boer and D G Pettifor (Amsterdam: Elsevier)
[5] Boykin T B, van der Wagt J P A and Harris J S 1991 *Phys. Rev.* B **43** 4777
[6] Di Carlo A and Lugli P 1995 *Semicond. Sci. Technol.* **10** 1673
[7] Schulman J N and Chang Y C 1985 *Phys. Rev.* B **31** 2056
[8] Zunger A, Yeh C-Y, Wang L-W and Zang S B 1994 *Proc. ICPS-22* p 1763
[9] Di Carlo A, Pescetelli S, Paciotti M, Lugli P and Graf M 1996 *Solid State Commun.* **98** 803
[10] Di Carlo A, Vogl P and Pötz W 1994 *Phys. Rev.* B **50** 8358
[11] Froyen S 1989 *Phys. Rev.* B **39** 3168
[12] Anderson E, Bai Z, Bischof C, Demmel J, Dongarra J, Du Croz J, Greenbaum A, Hammarling S, McKenney A, Ostrouchov S and Sorensen D 1992 *LAPACK User's Guide* (Philadelphia, PA: SIAM)
[13] Press W H, Flannery B P, Teukolsky S A and Vetterling W T 1986 *Numerical Recipes* (Cambridge: Cambridge University Press)
[14] Graf M and Vogl P 1995 *Phys. Rev.* B **51** 4940
[15] Priester C, Allan G and Lannoo M 1988 *Phys. Rev.* B **37** 8519
Priester C, Allan G and Lannoo M 1988 *Phys. Rev.* B **38** 9870
Priester C, Allan G and Lannoo M 1988 *Phys. Rev.* B **38** 13 451
Foulon Y and Priester C B 1991 *Phys. Rev.* B **44** 5889
[16] Reale A, Di Carlo A and Lugli P 1998 *VLSI Design* vol 8, p 469
[17] Di Carlo A, Reale A, Tocca L and Lugli P 1998 *IEEE J. Quantum Electron.* **34** 1730
[18] Hovinen M, Gopalan B, Johnson F G and Degenais M 1996 *Proc. IEEE Lasers and Electro-Optical Soc. Annu. Mtg (Boston, MA, 1996)* (New York)